Supporting Information

Bi-functional ionic liquids facilitated liquid-phase exfoliation of porphyrin-based covalent organic frameworks in water for highly efficient CO_2 photoreduction

Yingying Guo[1], Qian Zhang[1], Shuaiqi Gao[1], Huiyong Wang[1,*], Zhiyong Li[1], Jikuan Qiu[1], Yang Zhao[1], Zhimin Liu[2,*] and Jianji Wang[1,*]

[1]Key Laboratory of Green Chemical Media and Reactions (Ministry of Education), Collaborative Innovation Center of Henan Province for Green Manufacturing of Fine Chemicals, School of Chemistry and Chemical Engineering, Henan Normal University, Xinxiang, Henan 453007, P. R. China.

[2]Beijing National Laboratory for Molecular Sciences, Key Laboratory of Colloid, Interface and Thermodynamics, CAS Research/Education Centre for Excellence in Molecular Sciences, Institute of Chemistry, Chinese Academy of Sciences, Beijing 100190, China.

Table of Content

1. Hammett acidity function of ILs

Hammett acidity function of the ILs in water was determinded by an Uv-vis spectrophotometer (Elmer Lamda 35, Perkin -Elmer). Here, 4-nitroaniline (pK_a=0.99) was used as indicator. Firstly, the aqueous solution containing IL and 4-nitroaniline was prepared under stirring. The concentration of ILs and 4-nitroaniline in aqueous solution was 10 mmol L^{-1} and 13.5 μmol L^{-1}, respectively. Then the solution was kept under dark for 6 hours. The absorbance of solution was measured at the maximum absorption wavelength of 371 nm. The Hammett acidity function (H_0) of ILs was calculated by H_0=pKa(I)+lg([I]/[HI^+]), where I stands for indicator (4-nitroaniline), [I] and [HI^+] represent the concentration of protonated and unprotonated 4-nitroaniline, respectively. The value of ([I]/[HI^+]) can be determined from the absorbance value of solution. The computed values of the ILs was listed in Table S2. It was noted that since [HOEtMMIm]Cl, [HOEtMIm][NO_3] [NH_2PMIm]Br and [MIm]Cl can not provide [H^+] to 4-nitroaniline, the maximum absorbance of solution did not change and H_0 values could not be obtained.

2. Figures S1-S29

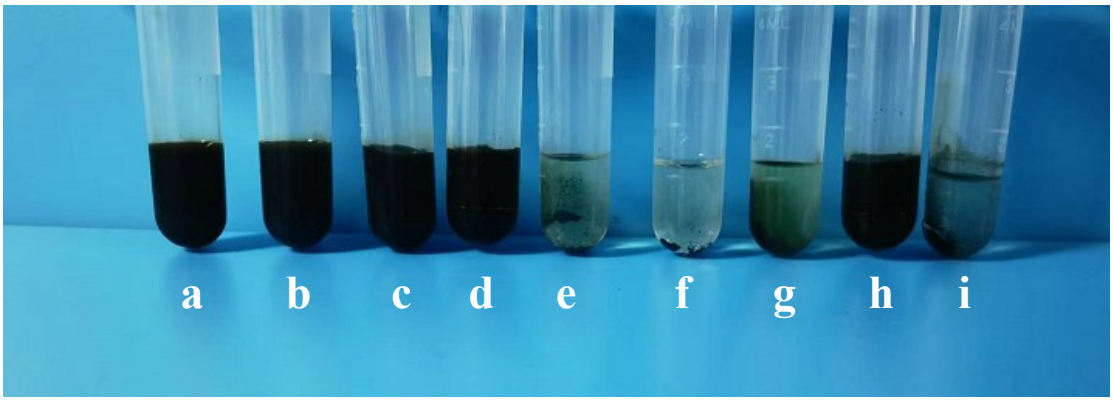

Fig. S1 Photos for the exfoliated 2,3-DhaTph CON in aqueous IL solutions: [HOOCMIm]Br (a), [$PrSO_3$HMIm]Cl (b), [HOEtMMIm]Cl (c), [HOEtMIm]NO_3] (d), [NH_2PMIm][BF_4] (e), [NH_2PMIm]Br (f), [Mim]Cl (g), [$PrSO_3$HPy]Cl (h), and [EPy]Cl (i).

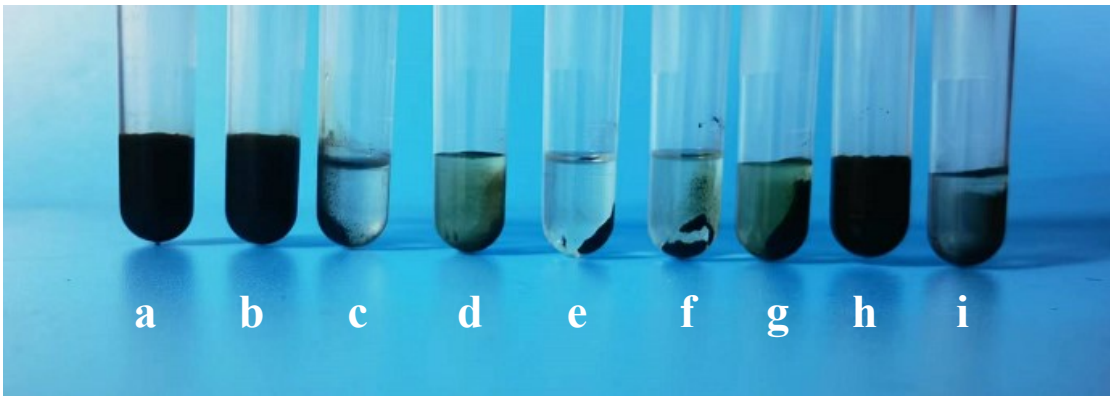

Fig. S2 Photos of the exfoliated 2,3-DmaTph CON in aqueous IL solutions: [HOOCMIm]Br (a), [$PrSO_3HMIm$]Cl (b), [HOEtMMIm]Cl (c), [HOEtMIm][NO_3] (d), [NH_2PMIm][BF_4] (e), [NH_2PMIm]Br (f), [Mim]Cl (g), [$PrSO_3HPy$]Cl (h), and [EPy]Cl (i).

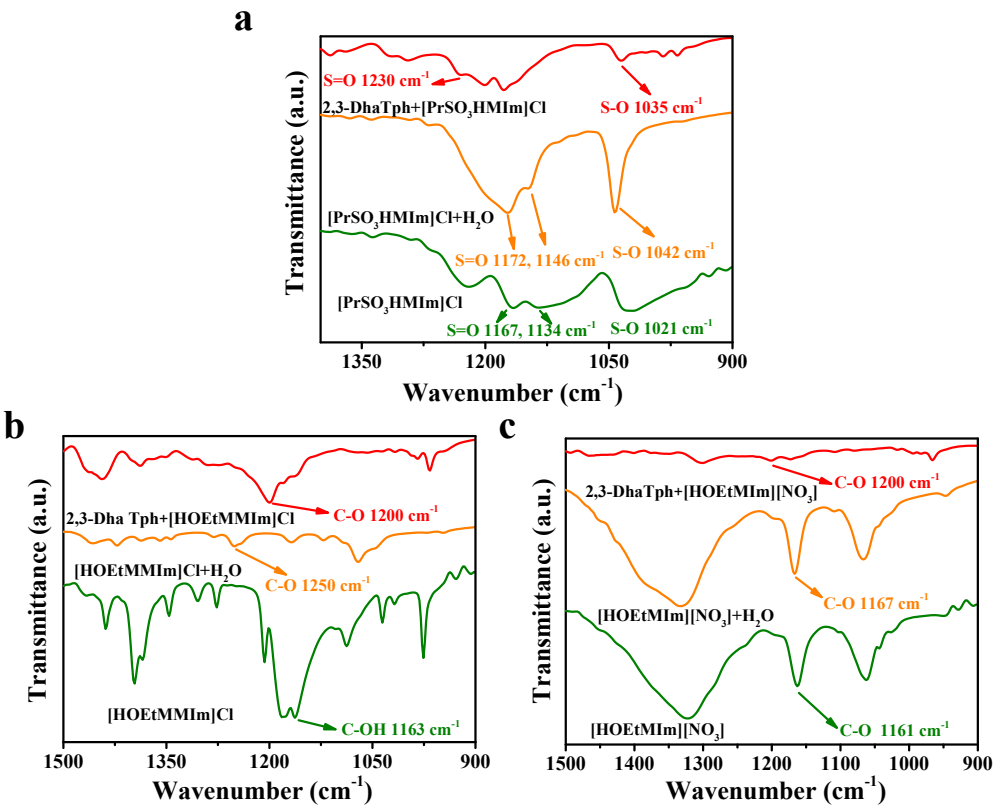

Fig. S3 FT-IR spectra of the ILs, the mixture of ILs with water (n_{COF}/n_{water}=1:1), and the mixture of ILs with 2,3-DhaTph COF (n_{COF}/n_{IL}=1:1): [$PrSO_3HMIm$]Cl (a), [HOEtMMIm]Cl (b), and [HOEtMIm][NO_3] (c).

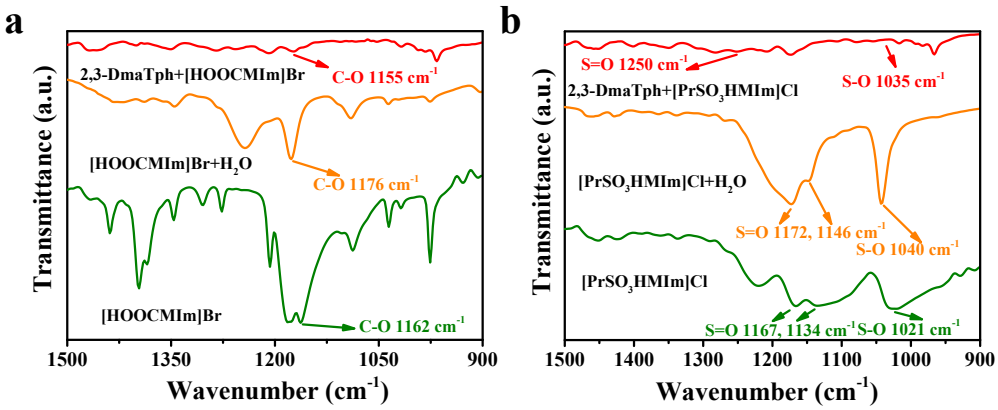

Fig. S4 FT-IR spectra of the ILs, the mixture of ILs with water (n_{COF}/n_{water}=1:1), and the mixture of ILs with 2,3-DmaTph COF (n_{COF}/n_{IL}=1:1): [HOOCMIm]Br (a) and [$PrSO_3$HMIm]Cl (b).

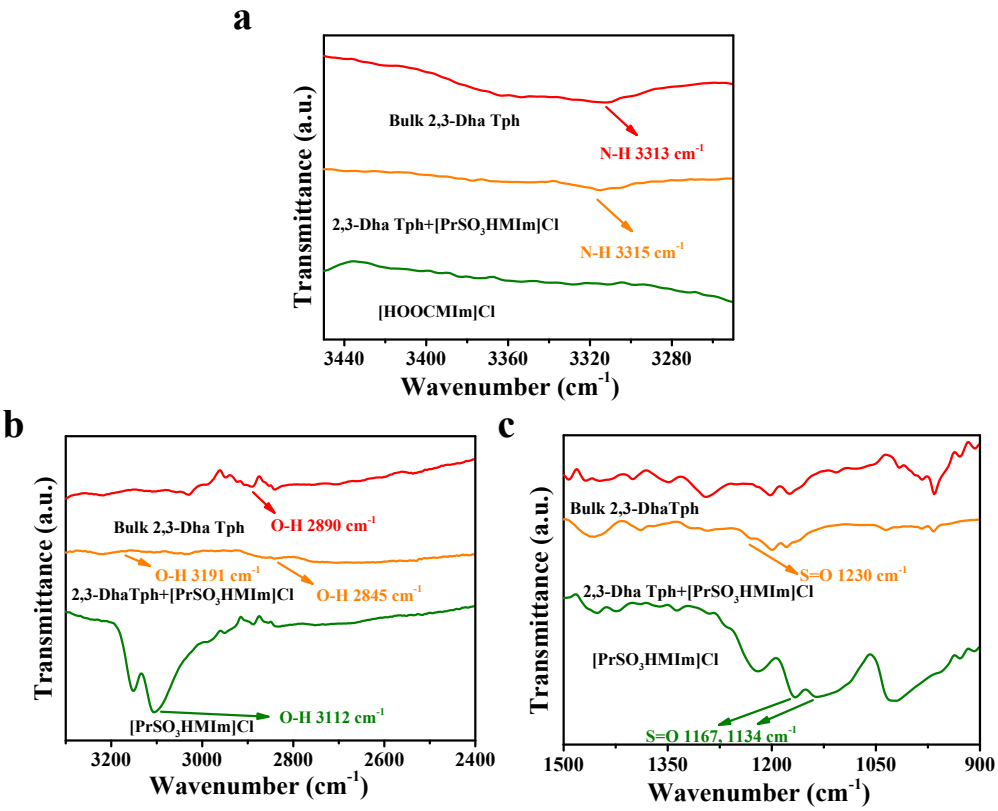

Fig. S5 FT-IR spectra of the bulk 2,3-DhaTph COF, [$PrSO_3$HMIm]Cl, and the [$PrSO_3$HMIm]Cl intercalated 2,3-DhaTph COF.

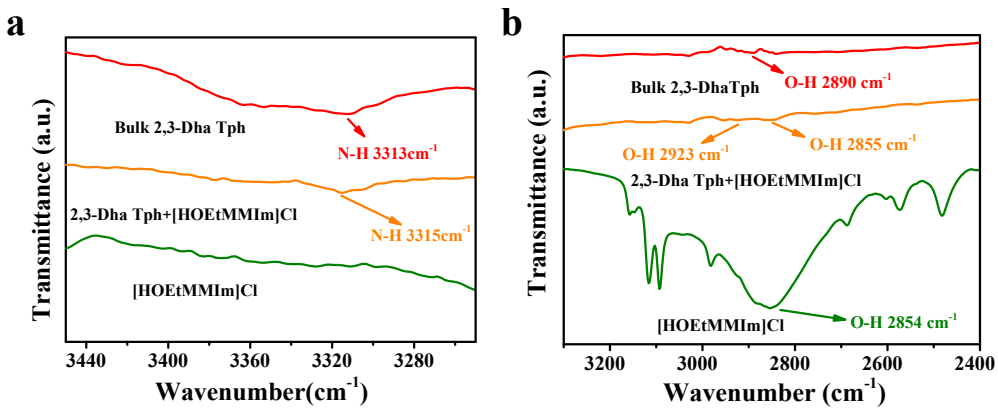

Fig. S6 FT-IR spectra of the bulk 2,3-DhaTph COF, [HOEtMMIm]Cl, and the [HOEtMMIm]Cl intercalated 2,3-DhaTph COF.

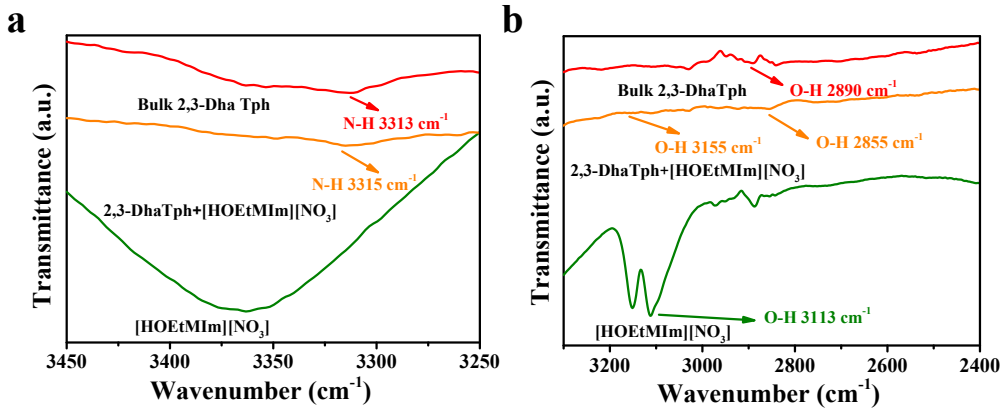

Fig. S7 FT-IR spectra of the bulk 2,3-DhaTph COF, [HOEtMIm][NO_3] and [HOEtMIm][NO_3] intercalated 2,3-DhaTph COF.

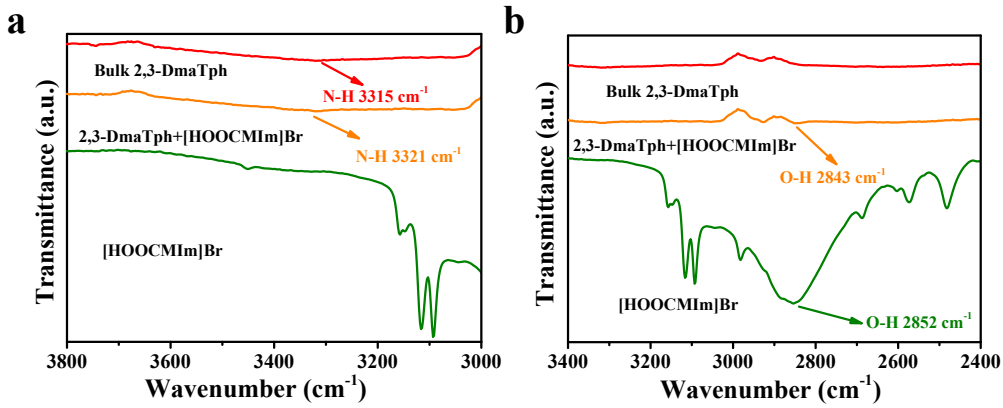

Fig. S8 FT-IR spectra of the bulk 2,3-DmaTph COF, [HOOCMIm]Br and [HOOCMIm]Br intercalated 2,3-DmaTph COF.

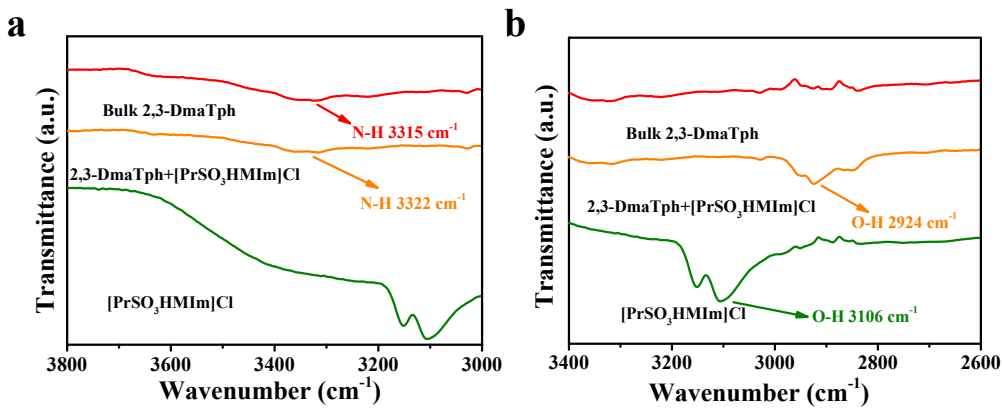

Fig. S9 FT-IR spectra of the bulk 2,3-DmaTph COF, [$PrSO_3HMIm$]Cl, and [$PrSO_3HMIm$]Cl intercalated 2,3-DmaTph COF.

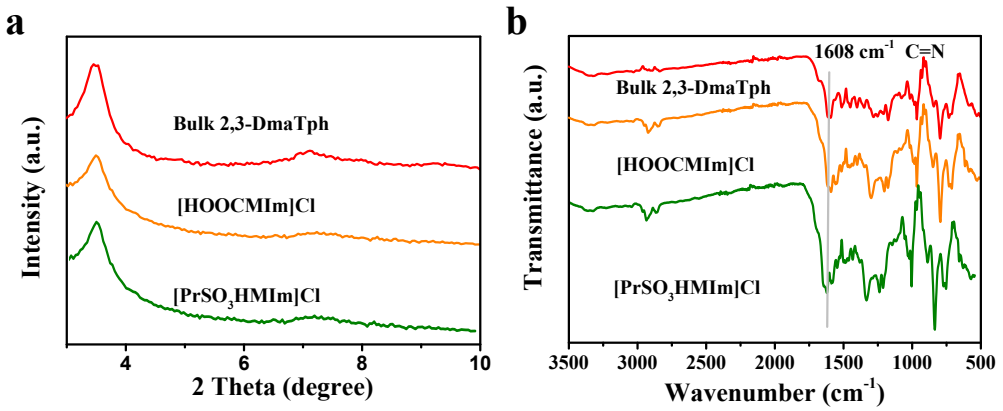

Fig. S10 XRD patterns (a) and FT-IR spectra (b) of the 2,3-DmaTph COF and 2,3-DmaTph CONs exfoliated in different aqueous ILs solutions.

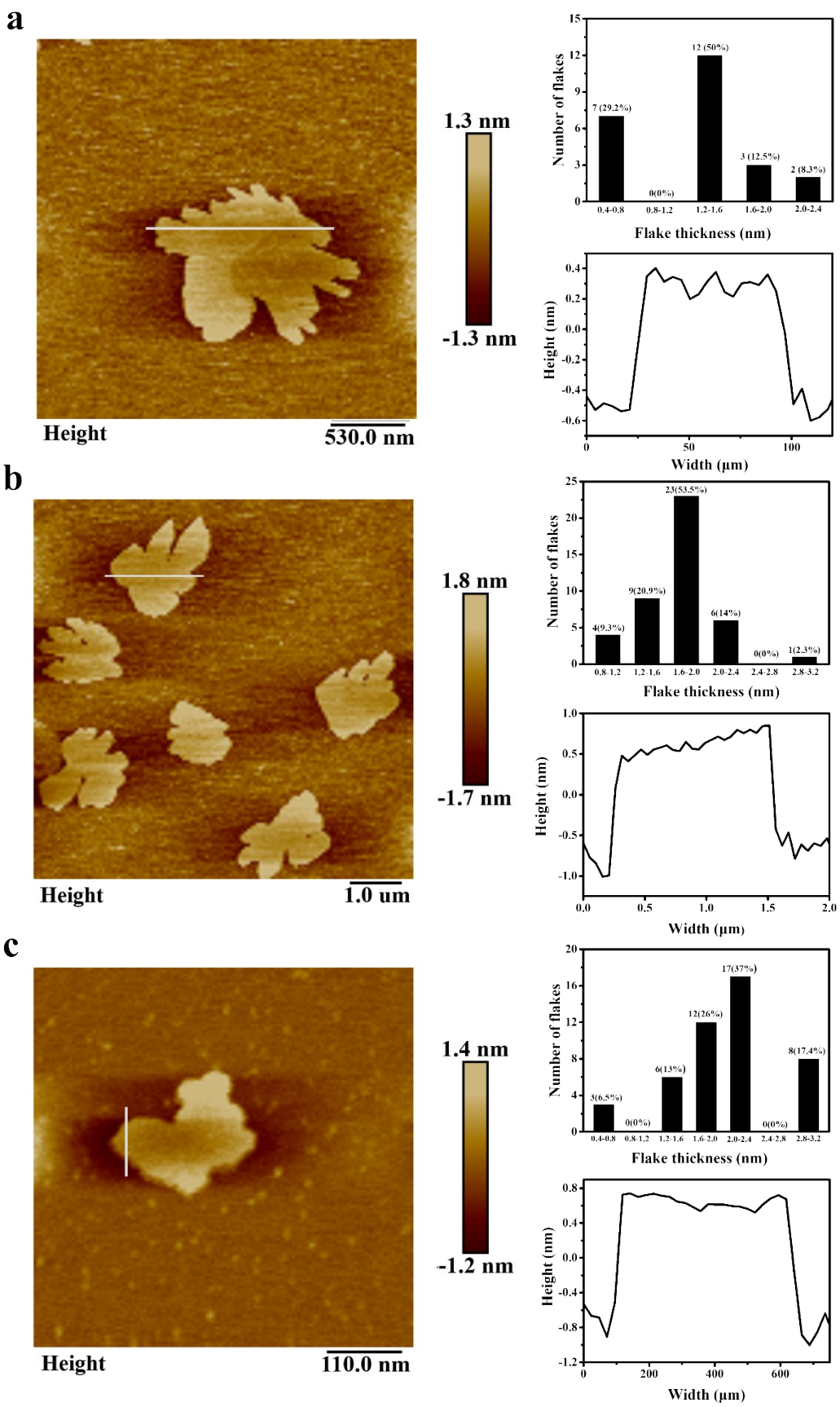

Fig. S11 AFM images of 2,3-DhaTph CONs exfoliated in water by [$PrSO_3HMIm$]Cl (a), [HOEtMMIm]Cl (b) and [HOEtMIm][NO_3] (c).

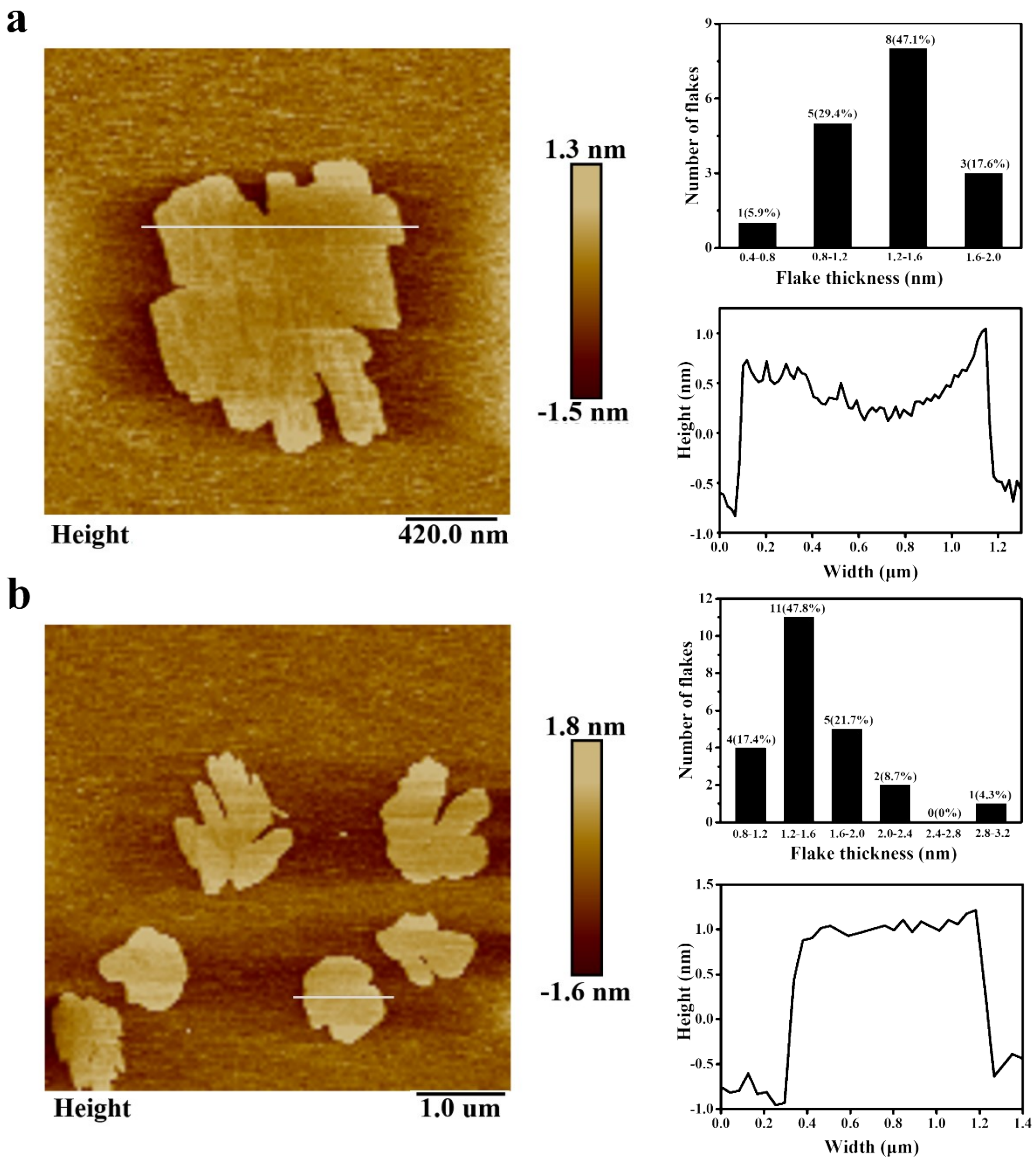

Fig. S12 AFM images of 2,3-DmaTph CONs exfoliated in water by [HOOCMIm]Br (a) and [$PrSO_3HMIm$]Cl (b).

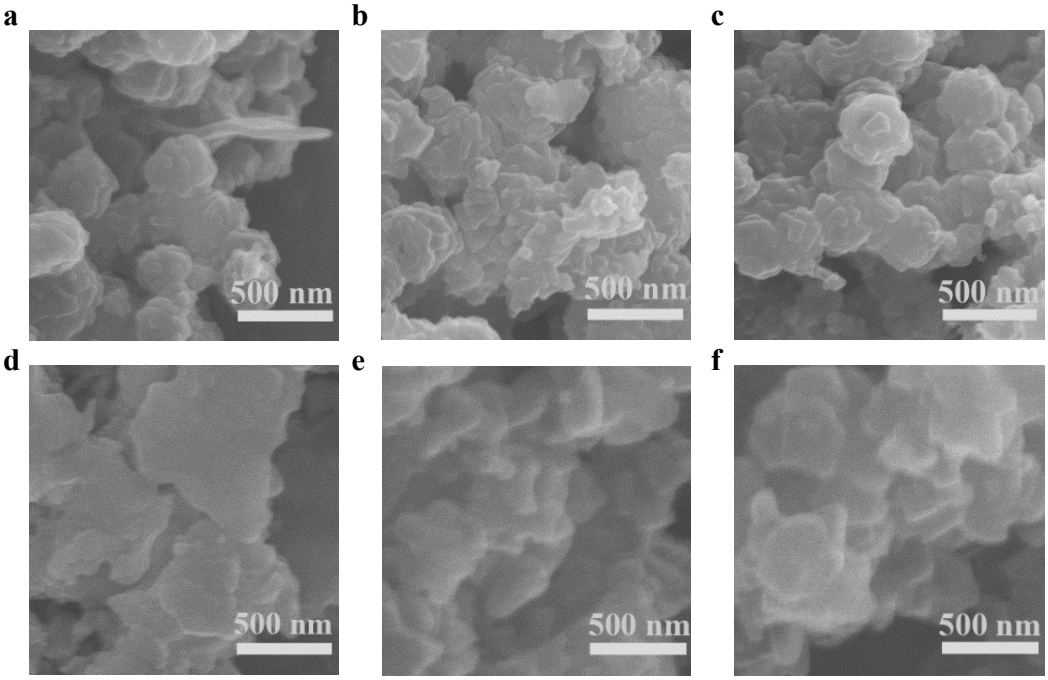

Fig. S13 SEM images of 2,3-DhaTph CONs exfoliated in water by [$PrSO_3HMim$]Cl (a), [HOEtMIm][NO_3] (b), [HOEtMMIm]Cl (c), and bulk 2,3-DmaTph (d), and 2,3-DmaTph CONs exfoliated in water by [HOOCMIm]Br (e), and [$PrSO_3HMim$]Cl (f).

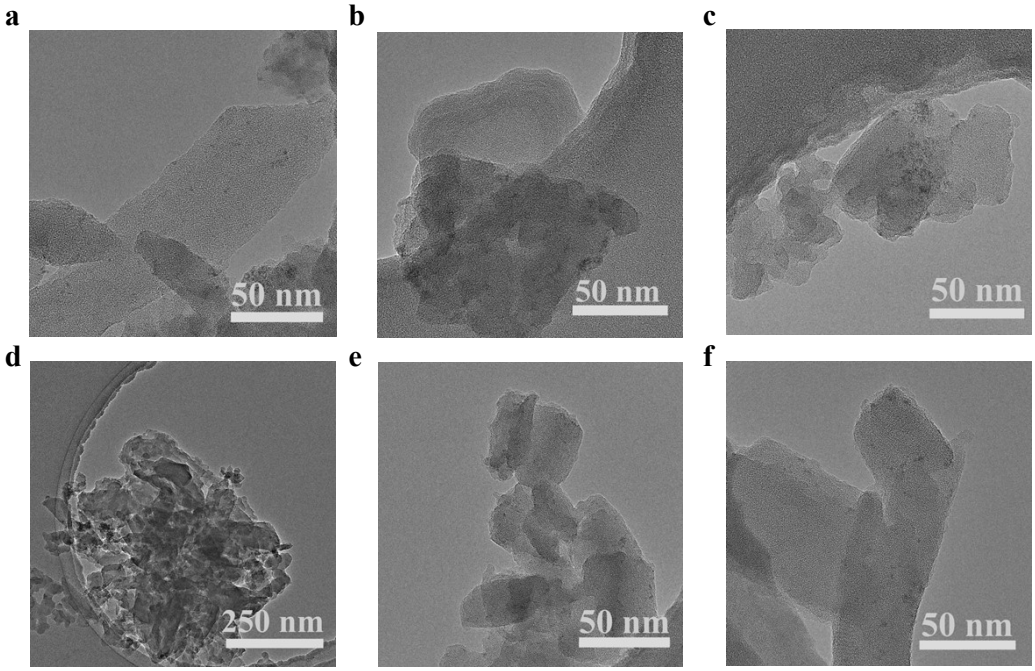

Fig. S14 TEM images of 2,3-DhaTph CONs exfoliated in water by [$PrSO_3HMim$]Cl (a), [HOEtMIm][NO_3] (b), [HOEtMMIm]Cl (c), and bulk 2, 3-DmaTph (d) and 2, 3-DmaTph CONs exfoliated in water by [HOOCMIm]Br (e), and [$PrSO_3HMim$]Cl (f).

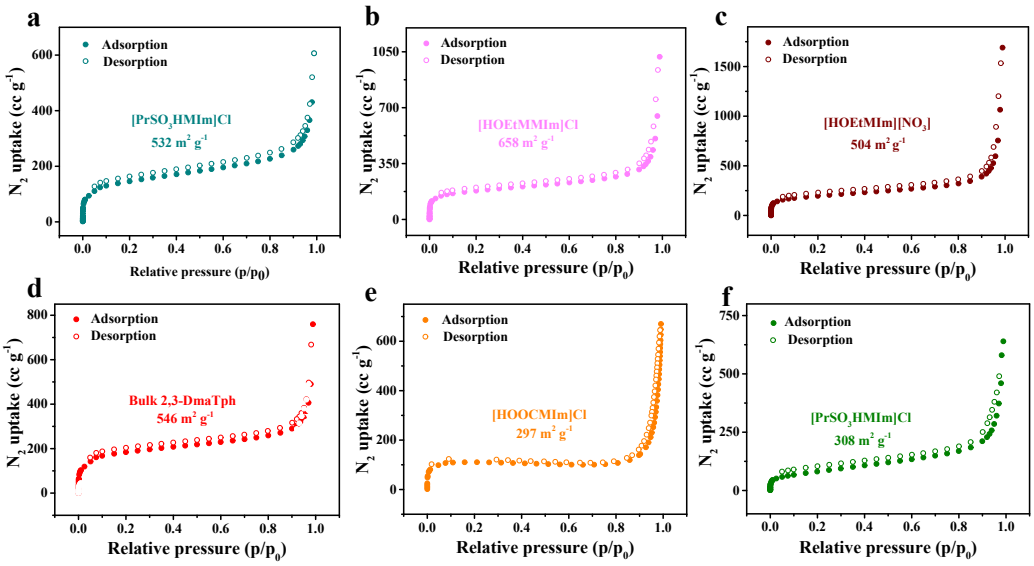

Fig. S15 N_2 absorption isotherms at 77K for 2,3-DhaTph CONs exfoliated in water by [$PrSO_3HMim$]Cl (a), [HOEtMMIm]Cl (b), [HOEtMIm][NO_3] (c), and bulk 2, 3-DmaTph COF (d) and 2, 3-DmaTph CONs exfoliated in water by [HOOCMIm]Br (e), and [$PrSO_3HMim$]Cl (f).

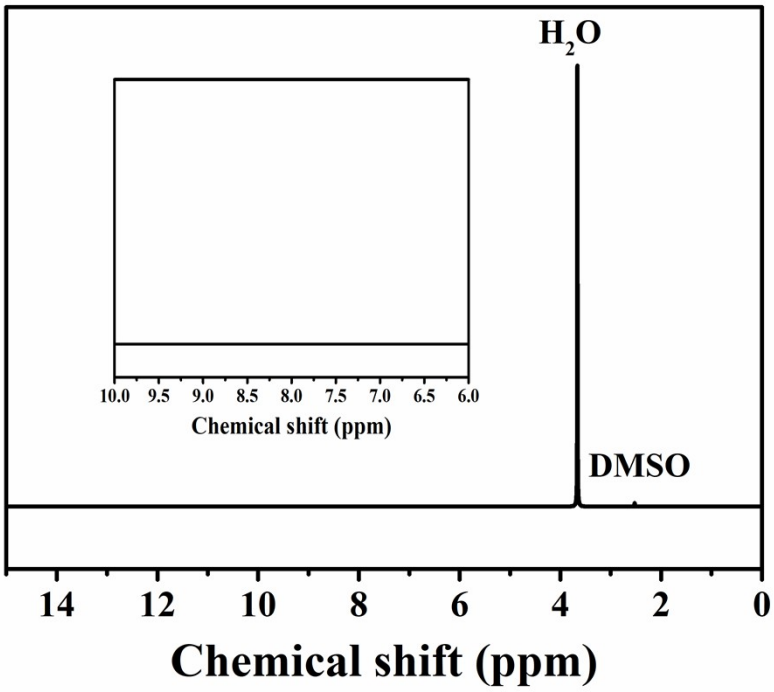

Fig. S16 ^{1}H-NMR spectra of the liquid products after a 4 h CO_2 photoreduction catalyzed by 2,3-DhaTph CONs. DMSO-d6 was used as the internal standard.

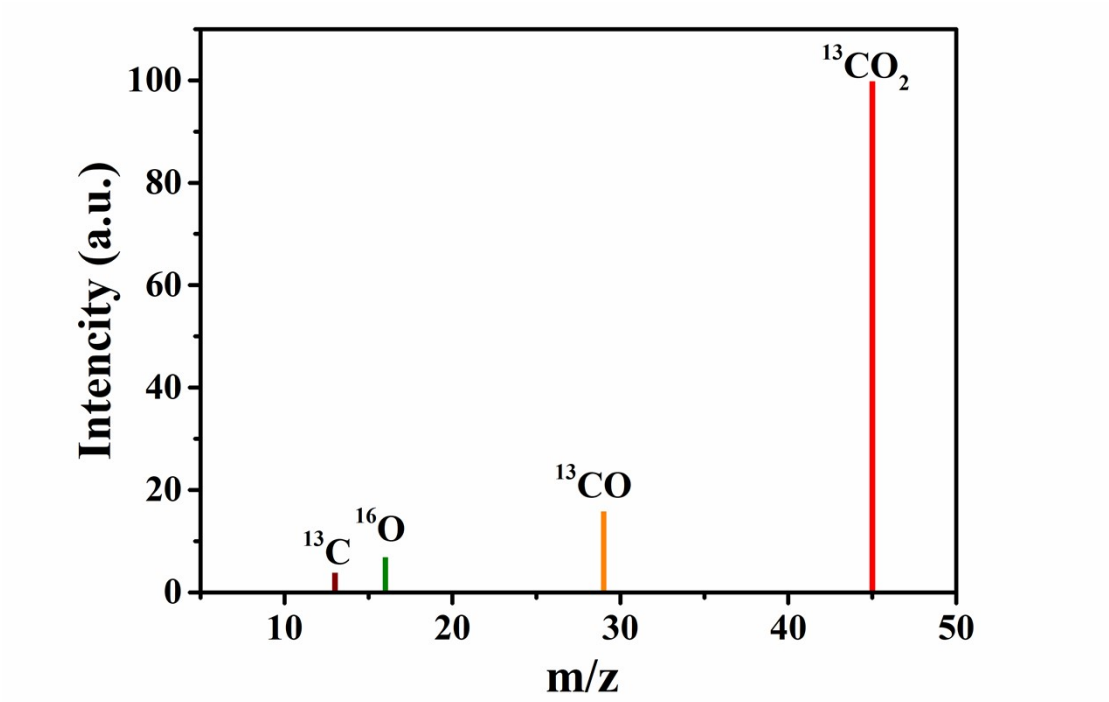

Fig. S17 ^{13}C isotope tracer tests based on GC-MS for 2,3-DhaTph CONs.

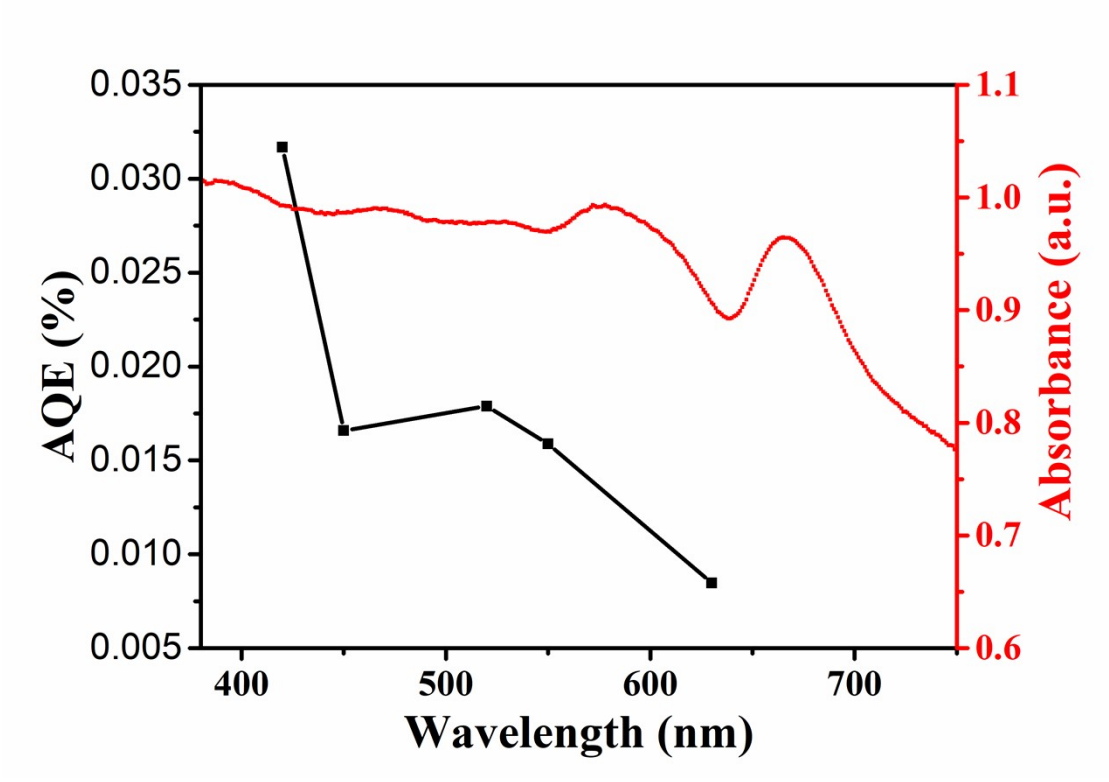

Fig. S18 The AQE of CO evolution at different wavelengths and the related UV-vis spectra catalyzed by 2,3-DhaTph CONs.

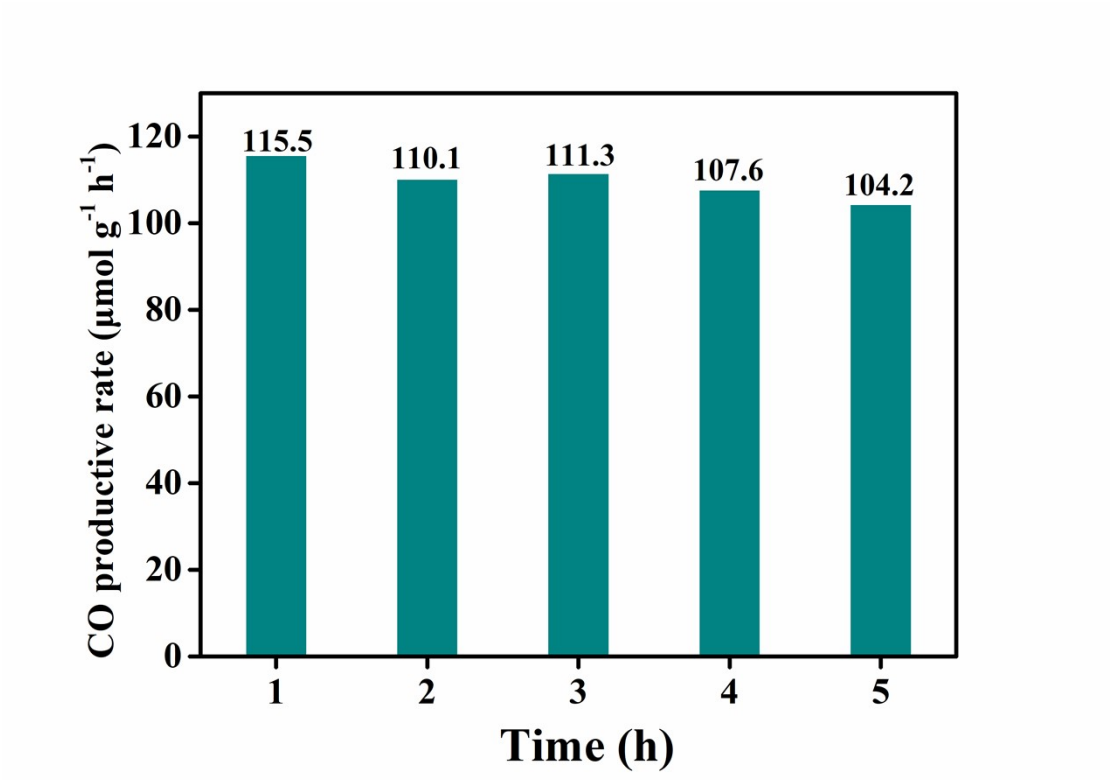

Fig. S19 Stability of 2,3-DmaTph CONs during 5 cycles of CO_2 photocatalytic reduction reaction to CO.

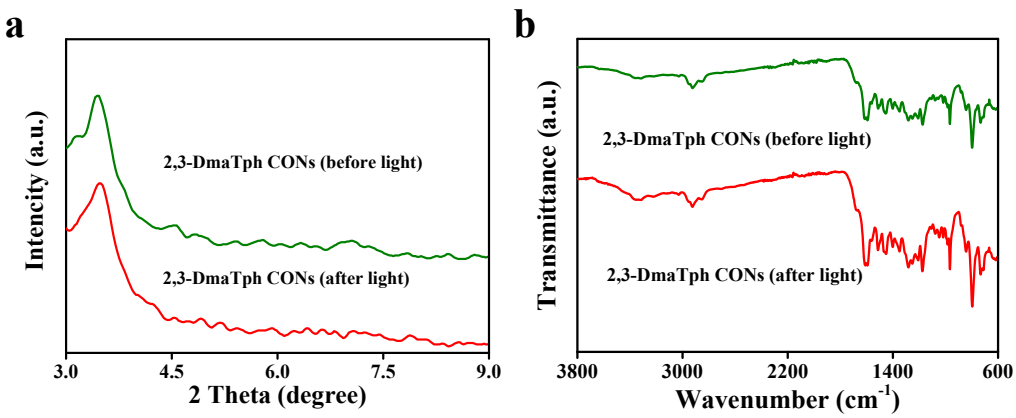

Fig. S20 XRD pattern (a) and FT-IR spectra (b) of 2,3-DmaTph CONs before and after photocatalysis reaction.

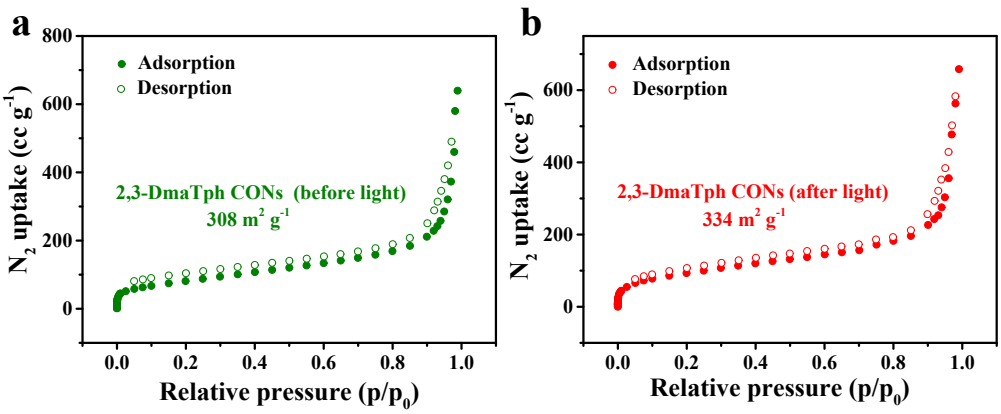

Fig. S21 N_2 absorption isotherms of 2,3-DmaTph CONs at 77K before (a) and after (b) photocatalysis reaction.

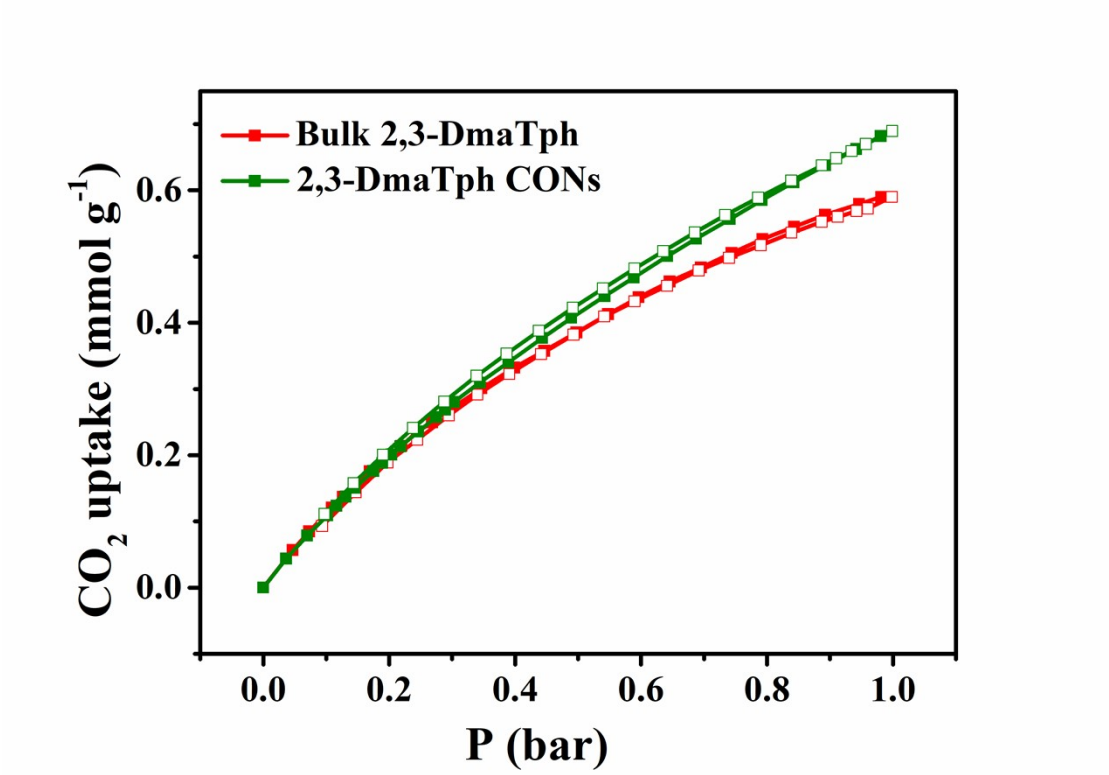

Fig. S22 CO_2 adsorption capacity of the bulk 2,3-DmaTph COF and 2,3-DmaTph CONs at 50 °C and 1 bar.

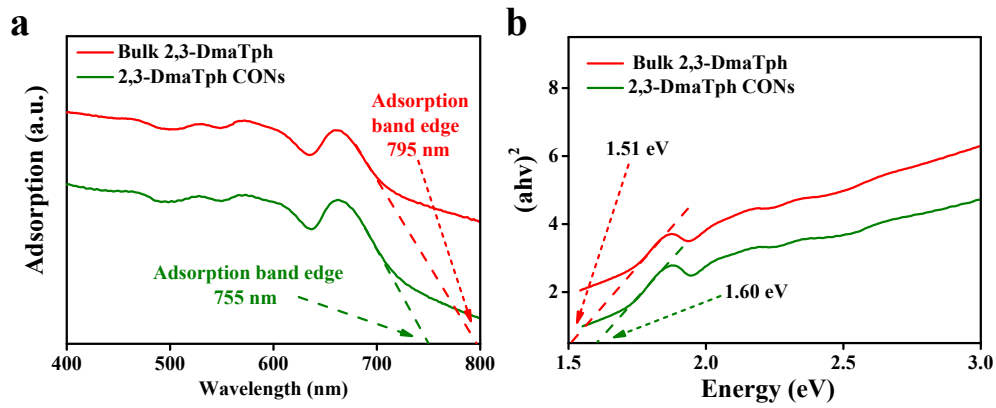

Fig. S23 Solid-state UV-vis diffuse reflectance spectra (a) and Kubelka-Munk-transformed reflectance spectra (b) of 2,3-DmaTph COF and 2,3-DmaTph CONs.

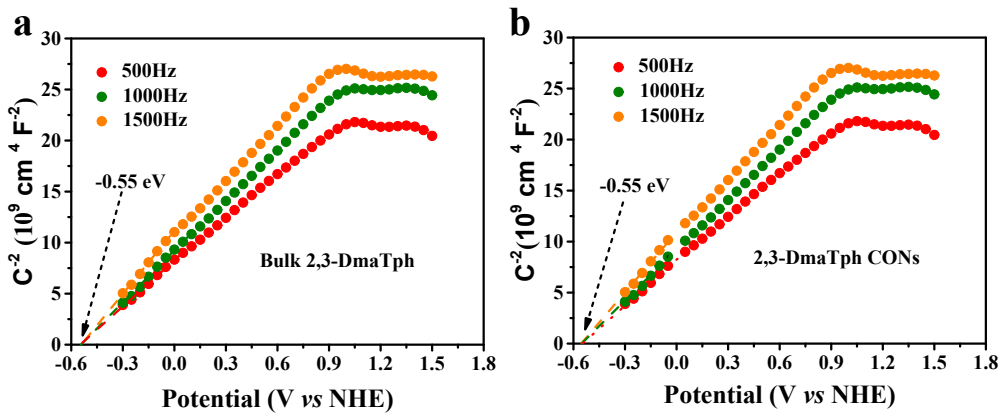

Fig. S24 Mott–Schottky plots and the calculated redox potentials for 2,3-DmaTph COF (a) and 2, 3-DmaTph CONs (b).

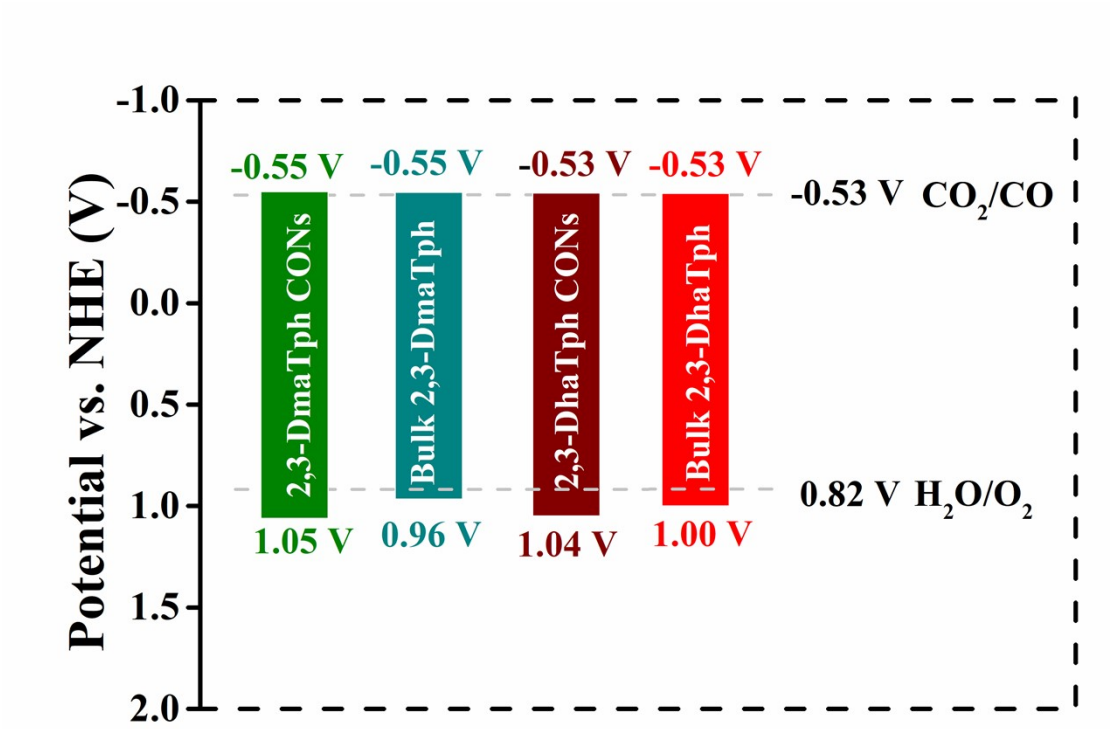

Fig. S25 Band structures of 2,3-DhaTph COF, 2,3-DhaTph CONs, 2,3-DmaTph COF, and 2,3-DmaTph CONs.

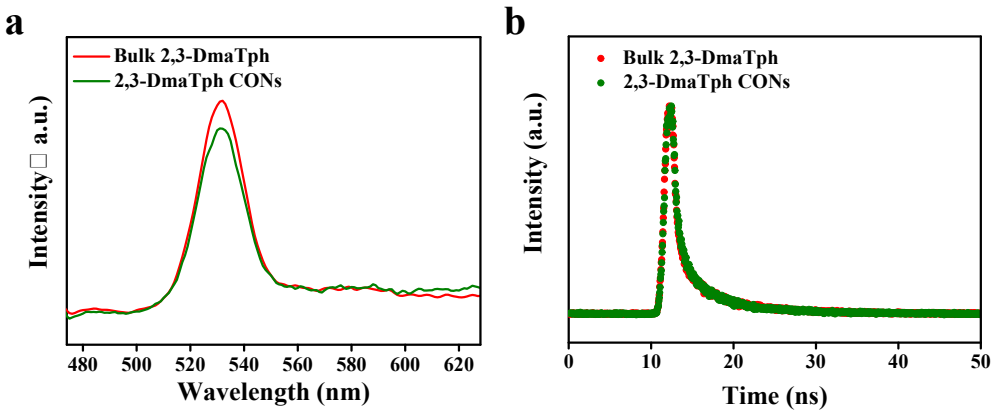

Fig. S26 Steady-state photoluminescent spectra (a) and time-resolved photoluminescent decay spectra (b) for 2,3-DmaTph COF and 2,3-DmaTph CONs.

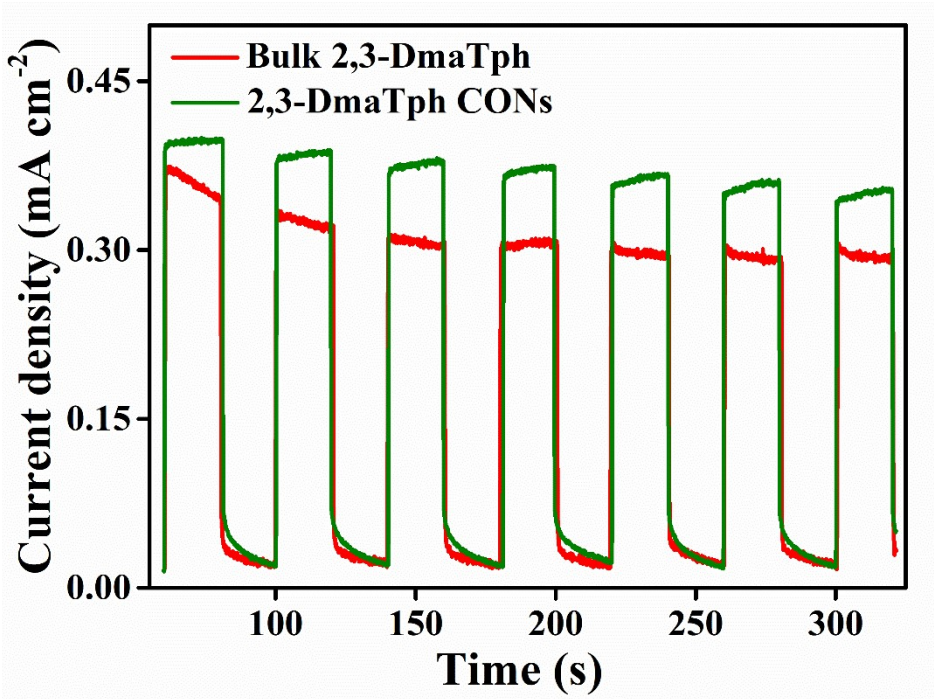

Fig. S27 Transient photocurrents of 2,3-DmaTph COF and 2,3-DmaTph CONs under xenon lamp (≥ 420 nm) irradiation.

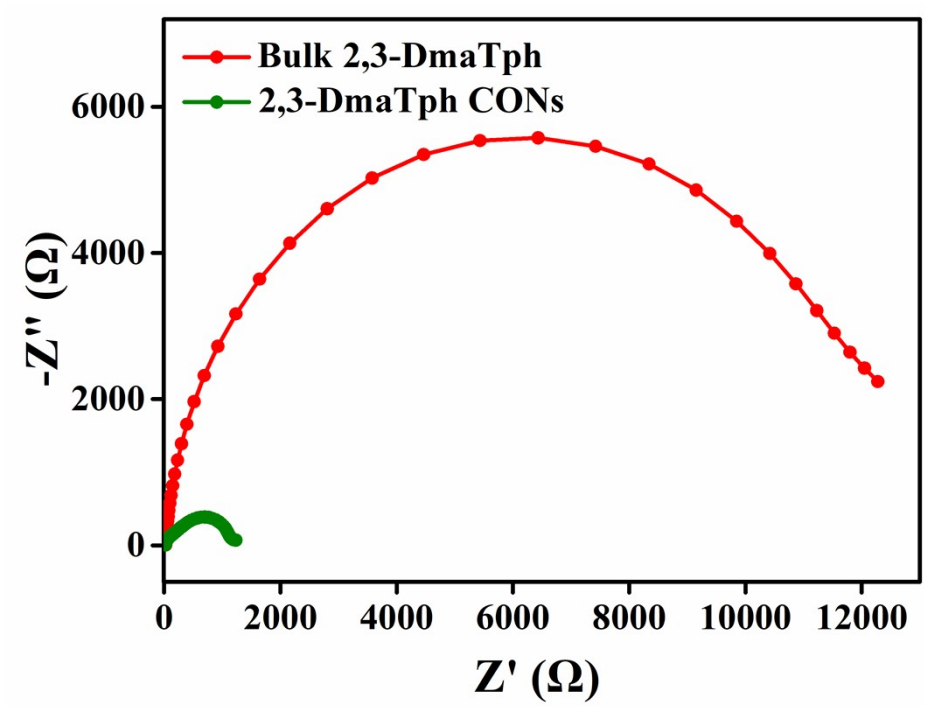

Fig. S28 Electrochemical impedance spectroscopy (EIS) for 2,3-DmaTph COF and 2,3-DmaTph CONs.

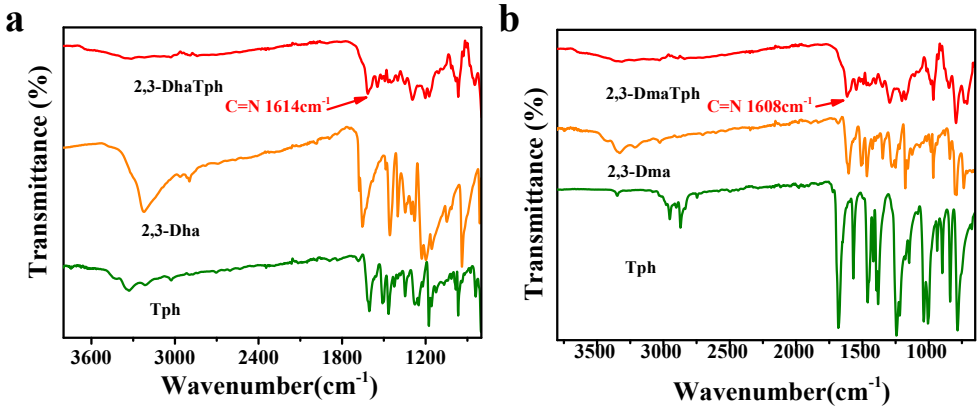

Fig. S29 FT-IR spectra of Tph, 2,3-Dha, 2,3-Dma, 2,3-DmaTph COF, and 2,3-DhaTph COF.

3. Tables S1-S4

Table S1 The original concentration and dispersion content of 2,3-DhaTph and 2,3-DmaTph in aqueous IL solutions under optimized conditions

COF	IL	Sonication power (W)	Sonication time (h)	Original concentration of COF (mg mL^{-1})	Content of CON (mg mL^{-1})
2, 3-DhaTph	[HOOCMIm]Br	400	8	3	1.82
2, 3-DhaTph	[$PrSO_3$HMIm]Cl	400	8	5	2.87
2, 3-DhaTph	[HOEtMMIm]Cl	400	8	5	1.93
2, 3-DhaTph	[HOEtMIm][NO_3]	400	8	5	1.76
2, 3-DhaTph	[$PrSO_3$HPy]Cl	400	8	5	2.83
2, 3-DmaTph	[HOOCMIm]Br	400	8	5	1.81
2, 3-DmaTph	[$PrSO_3$HMIm]Cl	400	8	5	2.33
2, 3-DmaTph	[$PrSO_3$HPy]Cl	400	8	5	2.24

Table S2 Hammett acidity function (H_0) values of the ionic liquids at 25 ^oC in water [a]

ILs	A_{max}	[I]%	[IH^+]%	H_0
blank	0.1806	100	-	-
[$PrSO_3$HMIm]Cl	0.1698	94.02	5.98	2.42
[HOOCMIm]Br	0.1742	96.42	5.98	2.18
[NH_2PMIm][BF_4]	0.1775	98.28	1.72	2.75

[a] A_{max} stands for the maximum absorbance of solution at 371nm, [I] and [HI^+] represent the concentration of protonated and unprotonated 4-nitroaniline, respectively.

Table S3 The Zeta potentials of 2,3-DhaTph and 2,3-DmaTph CONs dispersions at 25 ^{o}C

CON	IL	Zeta potential (mV)
2,3-DhaTph	[HOOCMIm]Br	57.1
2,3-DhaTph	[$PrSO_3$HMIm]Cl	51.3
2,3-DhaTph	[HOEtMMIm]Cl	43.3
2,3-DhaTph	[HOEtMIm][NO_3]	35.0
2,3-DmaTph	[HOOCMIm]Br	55.7
2,3-DmaTph	[$PrSO_3$HMIm]Cl	56.6

Table S4 The exfoliation yield of 2,3-DhaTph COF in aqueous [HOOCMIm]Br solution at different cyclic process

Number of cycles	Yield
1	66.6%
2	64.6%
3	59.3%
4	59.5%
5	57.5%
6	59.4%
7	54.5%
8	52.0%